

# EBSD and BKD

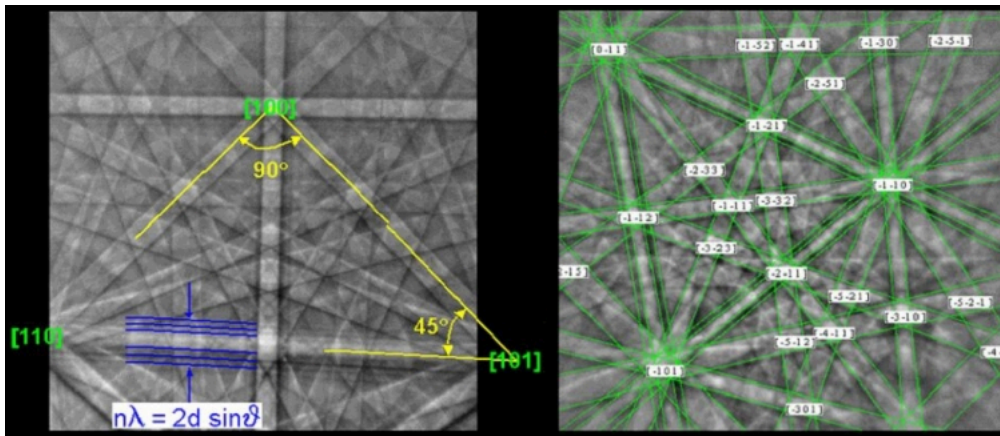
[Home](#)
[Basics](#)
[TKD](#)
[Radon vs Hough](#)
[FastEBSD](#)
[Conclusions](#)
[Publications](#)
[Downloads](#)
[Glossary](#)

## The evaluation of grain orientation data



### 1. Indexing of Kikuchi patterns

The characteristics of Kikuchi patterns are bands that are regularly arranged on a continuous background. They are delimited by straight lines. Strictly speaking, the edges of the Kikuchi bands are hyperbolas formed by the intersection of the Kossel cones with the plane of the detector. The intensity distribution in a Kikuchi pattern is not explained by a simple geometric model, but the dynamic theory of electron diffraction has to be employed [1]. The mechanisms that lead to the formation of the characteristic diffraction features in EBSD patterns, including Kikuchi bands as well as prominent circular Kikuchi envelopes around zone axes (by appearance like HOLZ lines from thin foils in CBED), have been explained, and excellent agreement has been obtained recently between experimental patterns and simulations in extended many-beam dynamical calculations using the Bloch wave approach [2].



For indexing it is sufficient to consider a pattern as a gnomonic projection of the crystalline lattice of the known phase on a plane detector. The point of impact of the stationary primary beam on the surface of the sample, or more precisely the volume of interaction in the grain, is the center of the projection. We can imagine that the planes of the lattice are stretched out until they cut the center lines of the associated Kikuchi bands. So, the angles between the center lines correspond to the interplanar angles. The "stars" at the crossings of the bands correspond to the axes of the crystal zones (see pattern on the left). The angular width of a band is equal to twice the Bragg angle  $\vartheta_{hkl}$ :

$$2d_{hkl} \sin \vartheta_{hkl} = n\lambda$$

whereby

$$\lambda = h / \sqrt{2 m q U} \approx \frac{6.6 \cdot 10^{-34} \text{Js}}{\sqrt{2 \cdot 9.1 \cdot 10^{-31} \text{kg} \cdot 1.6 \cdot 10^{-19} \text{C} \cdot U}} \approx \sqrt{\frac{1.5 \text{ V}}{U}} \text{ nm}$$

is a good approximation of the de Broglie wavelength of electrons at low to medium energy.

$d_{hkl}$  is the spacing between the lattice planes,

$n$  is the order of diffraction (integer),

$h$  is the Planck's constant,

$p$  is the momentum of the quantum particle (here the electron),

$m$  is the mass of the particle,

$q$  is the elementary charge of the particle,

$U$  is the acceleration voltage (measured in V).

A relativistic correction is necessary for accelerating voltages of about 100 kV and higher:

$$\lambda \approx \sqrt{\frac{1.5 \text{ V}}{U \cdot (1 + 0.98 \cdot 10^{-6} \cdot \frac{U}{V})}} \text{ nm} \approx \sqrt{\frac{1.5 \text{ V}}{U \cdot (1 + 10^{-6} \cdot \frac{U}{V})}} \text{ nm}$$

**Exercise:** Derive the rule of thumb for the wavelength of a free electron after passing through an acceleration voltage  $U$  from the De Broglie relation.  
 Calculate examples.  
 Download [Solution](#)

The convergence of the primary beam is not relevant. The extinction rules due to the structure factor of the crystal lattice apply for expected reflections (i.e. Kikuchi bands), and high order reflections may appear as a set of straight lines parallel to the band edges. The center line corresponds to the trace of the plane of the Bragg diffraction and thus seems to be strictly fixed to the lattice. This is, in addition to the sharpness of the lines, the basis of the high precision with which the orientation of a crystal can be determined.

The location of the Kikuchi lines, some of which are fractional, is difficult. They are extracted from the pattern by automated pattern recognition (see [Radon transform](#)). The localization of straight lines can thus be reduced to the search for isolated peaks in Radon space which stand for Kikuchi bands respectively Kikuchi lines.

Indexing is accomplished after provision of the positions of 5 to 10 narrowest and most intense bands of two or more zone axes of a pattern. The geometry of the pattern is compared with the positions of the lattice planes in the elementary cell. The calculation is carried out in computer programs that use look-up tables of the diffraction pattern families (tables of reflectors, interplanar angles and diffracted intensities) for the considered lattice system. With a multiphase material, the program tries to index the pattern with all the assumed crystal lattices. It accepts as true the solution and phase (phase discrimination) for which the backward calculated pattern (theoretical) best matches the measured pattern. Rough values for the geometric parameters (e.g. the position of the projection center = pattern center PC, the sample to screen distance = camera length  $L$ ) are needed at the beginning. They are refined by a least square fit between the actual and recalculated pattern. The crystallographic orientation of the grain is described either in  $(hkl)[uvw]$  notation, by three Euler angles  $(\varphi_1, \Phi, \varphi_2)$ , or by the rotation matrix  $g$ , which transforms the reference coordinate system of the considered sample into a coordinate system related to the crystal axes.

Finally, by simulating the pattern, it is verified that the grain orientation and the chosen crystal structure best fit the pattern. This check can also be illustrated by superposing the theoretical pattern on the experimental one (see pattern above on the right). The angular solution is limited by the precision with which the bands respectively lines can be localized in the pattern. Details of the indexing routine can be found for example in [3, 4]. Several commercial EBSD systems are available on the market.

[1] F.N. Chukhovskii, L.A. Alexanjan and Z.G. Pinsker: Dynamical Treatment of Kikuchi Patterns. *Acta Cryst.* **A29** (1973) 38-45

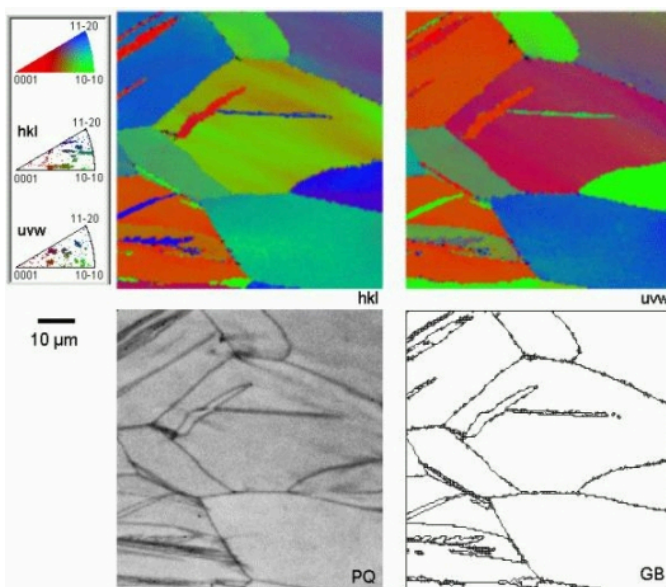
[2] A. Winkelmann: Dynamical simulation of electron backscatter diffraction patterns. in: A.J. Schwartz et al. (eds.): *Electron Backscatter Diffraction in Materials Science*, pp. 21-33. Springer Science+Business Media, NY 2009).

[3] P. Heilmann, W.A.T. Clark and D.A. Rigney: Computerized method to determine crystal orientations from Kikuchi patterns. *Ultramicroscopy* **9** (1982)365-371

[4] [Download](#)  R.A. Schwarzer: Review Paper: Automated crystal lattice orientation mapping using a computer-controlled SEM. *Micron* **28** (1997) 249-265.

## 2. Pattern Quality PQ - an indication of the imperfection of the lattice

### A Pattern Quality Map PQ reveals grain structure



hkl and uvw orientation, pattern quality and grain boundary maps of a rolled Ti specimen.

### The determination of pattern quality PQ

- Measure height of "butterfly" peaks resp. peak profile.
- Measure slope of Kikuchi band edges.
- Sharp contours correspond to high spatial frequencies in the Kikuchi pattern  
 => Fast Fourier Transform (FFT) and frequency analysis.
- Special case: low dislocation density and high spatial resolution:  
 => measure microshifts and slight rotations of bands in successive patterns of a grain.  
 => automated approach by evaluating correlation function of successive patterns.
- 2D FFT of the whole initial backscatter Kikuchi pattern (Krieger Lassen, 1994):
  - Measures in all polar directions with equal weights.
  - Picks up pixel noise which has almost the same spatial frequencies as the band contours.
  - Is too slow.
- 1D FFT along  $\rho$  direction in Radon space - [1, 2] making use of Fourier slice theorem (Morneburg, 1995): (1D FFT of RT  $\sim$  2D FFT of the original image)
  - + RT averages off statistical pixel noise.
  - +  $\rho$  direction is perpendicular on each band = slope of

band edges.

+ Extracts the fine structure of the bands.

+ 1D FFT is fast, RT has already been calculated for band tracing.

[1] J. Sukkau and R.A. Schwarzer: Reconstruction of Kikuchi patterns by intensity-enhanced Radon transformation. *Pattern Recognition Letters* **33** (2012) 739–743.

[2] R.A. Schwarzer and J. Sukkau: Automated evaluation of Kikuchi patterns by means of Radon and Fast Fourier Transformations, and verification by an artificial neural network. *Adv. Eng. Mat.* **5** (2003) 601–606.

### 3. Orientation Microscopy

The prime objective of orientation microscopy is the acquisition of grain orientation data. They are usually represented by three Euler angles or by the rotation matrix which rotate the coordinate system of the specimen in the coordinate system fixed to the particular crystal lattice.

A clear graphical representation of the microstructure is obtained by constructing Crystal Orientation Maps (COM), or in short Orientation Maps (OM) [1]. Hereby the orientation parameters in the measured grid points are assigned in an image to unique shades of three basic colors that are red, green and blue. Orientation parameters in crystal orientation maps may be two crystallographic directions (hkl)[uvw] for two sample reference directions ("Miller maps"), the Euler angles ( $\varphi_1$ ,  $\Phi$ ,  $\varphi_2$ ) ("Euler maps"), or the Rodrigues vector R ("Rodrigues maps"). Finally an orientation map of the sample is obtained which illustrates the morphology of microstructure and the spatial orientation distribution of the grains. If abutting points in a region have the same or similar orientations as their neighbors, they are identified as a grain, and the intersections of such regions are called grain respectively phase boundaries. Grains with an orientation closely in common are represented by similar colors. It is so possible to quantitatively represent the orientations and misorientations in materials on the sub-micron scale.

The misorientations between neighboring raster points are calculated and, by assuming specified threshold values, grain boundaries (GB) as well as phase boundaries can be marked out in the COM. However, a grain boundary in a planar sample section forms a closed perimeter line which must not "leak". A special "path finding" algorithm along the grain boundary segments is applied to fill missing spots where indexing may have locally failed, and a (binary) grain boundary network of the microstructure is obtained. The lines may be further skeletonized to one pixel in width. Grain boundaries are commonly marked by the Rodrigues vector, R, the axis-angle parameters of the misorientation,  $\Delta g$ , or the  $\Sigma$  character according to the CSL model. Other local properties or parameters can be represented graphically by color maps of the microstructure in a similar way, such as dislocation density, the predominant glide systems or twin systems in the grains, the Schmid factor or the residual deformation energy in the individual grains [2].

The advantages of grain-boundary COM over conventional light microscopical images of grain boundary networks are for stereological evaluation:

+ The grain-boundary COM is based quantitatively on measured crystallographic orientations rather than on tricky methods of surface (GB) etching and imaging.

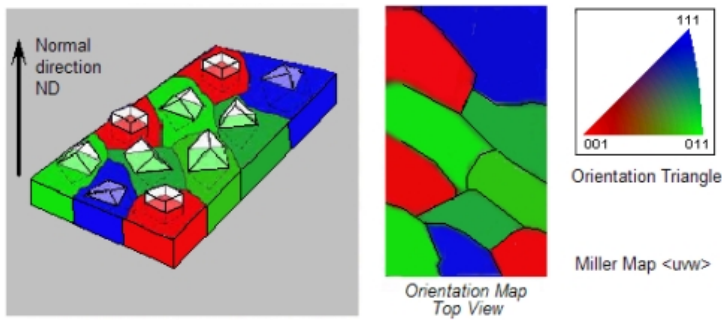
+ A high contrast on a flat background is obtained over the whole grain-boundary COM due to a yes/no discrimination of intensity levels.

+ The data are available in a digital (binary) format on a regular raster grid.

Therefore, standard methods of quantitative metallography can directly be applied to skeletonized grain-boundary COM. In many labs sophisticated stereological programs are already available. 2D microstructure parameters can so be determined such as the area fraction, planar size, average grain size, shape and arrangement of grains, and their statistical distributions. If the phases in the material have sufficiently different lattice constants or differ in their element composition so that the phases can be differentiated - with the aid of simultaneous EDS analysis - in every pixel, quantitative metallography can be extended to a phase discriminating stereology. Under usual stereological assumptions, 2D stereology is often extended to 3D stereology to calculate such parameters as volume fraction, average grain volume, 3D shape and arrangement, contiguity of phases, and their statistical distributions. Approaches are made to reveal the true 3D microstructure on a grain specific scale by combining BKD with in-situ serial sectioning in a FIB&SEM instrument.

Since a grain in the grain-boundary COM is represented by the group of pixels with similar grain orientations within the GB loop, its area fraction is simply measured by counting the raster points which are enclosed by the grain boundary perimeter line. This point-counting method is superior over the line-intercept method because it is not affected by concave sections of the grain boundary line nor by "islands" formed by a second grain underneath which may shine through the sample surface. A rapid but less precise alternative for estimating size and shape of grains is the visual comparison of a grain-boundary COM with standard grain charts or reticules.

For orientation maps using Miller indices as orientation parameters, a color triangle is overlaid on the stereographic standard triangle of the crystal lattice under consideration [1]. In case of cubic crystal symmetry red is commonly assigned to directions near the (001) corner, green to directions near the (011), and blue to the directions near the (111) corner. Using this legend, colored Miller maps provide an illuminating display of the spatial and angular distribution of crystallographic directions related to reference directions in the sample, for instance the sheet normal direction, ND, and the rolling direction, RD, in rolled sheets. Two Miller maps are required, one for the {hkl} in-surface planes (i.e., in case of cubic symmetry the  $\langle hkl \rangle$



directions perpendicular on the specimen surface), and one for the  $\langle uvw \rangle$  in a reference direction in the specimen surface, to fully represent the grain orientations in the surface. When both Miller maps are considered, the spatial and angular distribution of crystallographic orientations is clearly visualized.

The unique colors, on the other hand, can be interpreted in terms of orientation parameters by comparison with a color legend. The full grain orientation may be reconstructed from a set of two colored Miller maps in

the following way: From the symmetrically equivalent orientations only those have been used for imaging whose Miller indices (hkl) of the in-surface planes fall in the standard triangle 001-011-111. One of the permutations of the Miller indices, [uvw], of an orthogonal direction is given in the standard triangle 001-011-111. For a full description of crystal orientation the sign and sequence of the Miller indices [uvw] is determined considering the condition of orthogonality between (hkl) and [uvw]. If this condition is fulfilled for more than one of the permutations of  $\langle uvw \rangle$ , these solutions are symmetrically equivalent. They cannot be discriminated physically from each other, because the choice of the position of the axes of the elementary lattice cell is arbitrary.

It is worth noting that conventional light or scanning electron microscopy images may display abutting grains by the same color or gray shade. Therefore, Quantitative Metallography may fail when deriving grain size distributions or other statistical parameters from microscopy images. In crystal orientation maps, however, grains (and phases) are discriminated unambiguously by indicating their crystal orientation and lattice structure. Since crystal orientation maps are available in digital form by their way of construction, the derivation of statistical parameters (such as the distributions of grain size, length of grain boundaries, grain size as a function of grain orientation, and the fractions of  $\Sigma$  grain boundaries) is simply reduced to pixel counting.

[1] [Download](#)  D. Gerth and R.A. Schwarzer: Graphical representation of grain and hillock orientations in annealed Al-1%Si films. *Textures and Microstructures* **21** (1993) 177-193

[2] [Download](#)  R.A. Schwarzer: Review Paper: Automated crystal lattice orientation mapping using a Computer-controlled SEM. *Micron* **28** (1997) 249-265

#### 4. Pole Figures and ODF

The Orientation Density Function (ODF) and pole figures can be constructed directly from a data set of individual grain orientations by associating the orientations or the volume fractions of grains having these orientations with points or discrete cells of finite size in the Euler orientation space, on pole figures (stereographic projection) or on inverse pole figures (standard triangle of the crystal symmetry group). With increasing number of data points such discrete representations are difficult to survey. So they are often normalized, smoothed, filtered and converted to equal density line representations, or the densities are scaled to color intervals in the plots of ODF sections, pole figures or inverse pole figures. This method of discrete representation appears easy and straightforward, but has drawbacks even if the Euler plots and Pole Figure Plots are smoothed and normalized to equal densities. First, the distortions of the Euler space for small  $\Phi$  angles are usually not taken into account (nor the distortions of the stereographic projection) since for simplicity the Euler space is subdivided into cells of constant angular increments. Second, the number of measured orientations is often not high enough to guarantee statistical relevance.

An elegant approach to smooth and to condense the data set into a continuous representation is the calculation of the ODF,  $f(g)$ , by series expansion into generalized spherical harmonics (T functions) after Bunge [1]:

$$f(g) = \sum_{l=0}^L \sum_{m=0}^M \sum_{n=0}^N c_l^{mn} T_l^{mn}(g)$$

The expansion coefficients (termed "C coefficients") are then expressed by

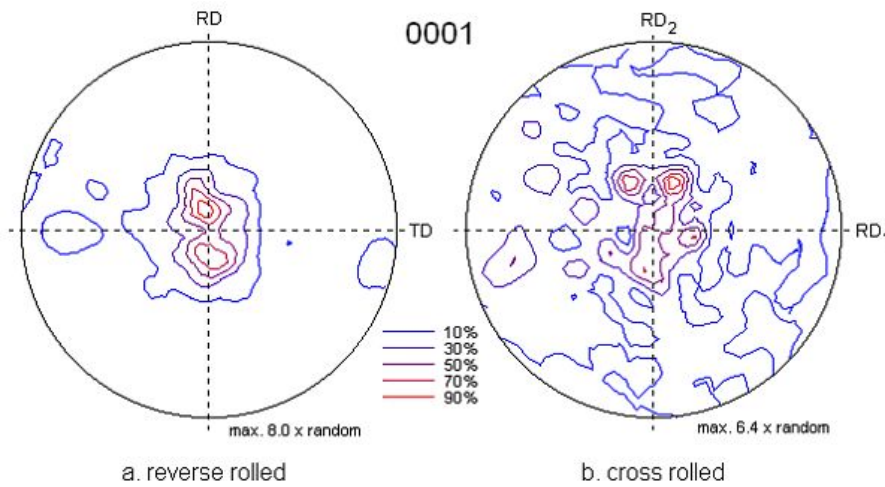
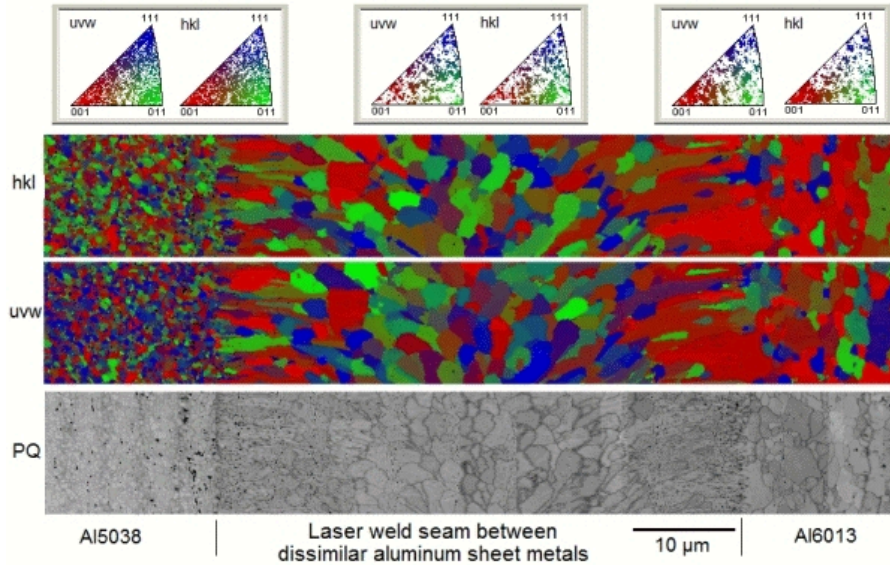
$$c_l^{mn} = \sum_{s=1}^S K_s(l) \cdot V_s \cdot T_l^{mn}$$

$V_s$  stands for the volume fraction of grain  $s$ , and  $K_s(l)$  for the convolution kernel of the expansion. Common convolution kernels are a Dirac  $\delta$  function in case of a large number  $S$  of orientations, or Gauss type distributions in Euler space with a half width  $\Psi_{0s}$  at  $1/e$  maximum of the Gauss peak at the orientation point  $g_s$  [2, 3]

$$K_s^{Gauss}(l) = \frac{\exp(-l^2 \Psi_s^2) - \exp(-(l+1)^2 \Psi_s^2)}{1 - \exp(\Psi_s^2)}$$

The C coefficients are a highly concise and convenient description of crystal texture. They enable the calculation of normal and inverse pole figures, important elastic and plastic materials properties, and tensorial properties in general [1]. ODFs calculated from EBSD and from X-ray pole figure measurements usually agree very well if the data have been acquired on the same specimen area.

N.B.: In X-ray diffraction, the reflections and hence pole figures are indexed according to their diffracting lattice planes  $\{hkl\}$ . By tradition, inverse pole figures referred to the specimen surface are also indexed according to the in-surface lattice planes rather than to the crystallographic directions perpendicular to the specimen surface. This inconsequent definition is of no relevance in case of cubic crystal symmetry, but has to be kept in mind when studying materials of lower symmetry.



0001 pole-figures of a cross-rolled AM20 magnesium sheet.  
Initial thickness of the hot extruded material was 7 mm.

The sheet metal was clockwise cross-rolled in steps of  $90^\circ$  with 200 mm/s in 17 stitches down to 0.95 mm. The rolls were kept at  $100^\circ\text{C}$ . Between the rolling steps, the samples have been annealed (recrystallized) at  $420^\circ\text{C}$  for 20 min. (1.7-2.5 wt% Al, min. 0.2 wt% Mn, max. 0.2 wt% Zn, balance Mg)

*You should keep in mind:*

- The ODF is only partially suitable for predicting the properties of engineering materials. The ODF is an idealizing model of the polycrystalline solid that reflects only the volume fraction statistics respectively the numbers of crystal orientations in the measured sample. It completely ignores the stereology of the microstructure, i.e. in particular the location of crystallites, the size of individual grains, their size distribution in the microstructure, their relationship and interaction with their neighborhood, grain boundaries and phase joints, joint properties, and the sub-microstructure (e.g. dislocations, stacking faults and inclusions). The ODF, calculated from the pole figure inversion, is not unique, but depends on the calculation method.
- Amorphous phases are not detected in the pole figure measurement.
- The Eulerian space has a very distorting metric. The ODF representation in Eulerian space therefore easily leads to misinterpretations when considering the usual 3D Cartesian representation. The distortion for pole figures in the usual stereographic projection must also be considered.

- + From EBSD data, however, the ODF can be constructed unambiguously by writing the measured volume-weighted or number-weighted orientation of the crystallites, for example in 3D Eulerian space.
- + This ODF can then be compared to the results of current measurements (conventional pole figure measurement by X-ray diffraction, synchrotron or neutron) or to historical measurements from the literature.
- + The ODF in serial development according to Bunge is a very compact summary. When the textures are not too flat, a few development coefficients are often sufficient for useful texture characterization and material property estimation.

[1] H.-J. Bunge: Texture analysis in materials science - Mathematical methods. Butterworths, London 1982 (ISBN 0-408-10642-5)

[Download](#)  Paper back reprint: Cuvillier-Verlag Göttingen 1993 ( ISBN 3-928815-81-4)

[2] F. Wagner: Texture determination by individual orientation measurements. In: Experimental Techniques of Texture Analysis, H.J. Bunge (ed.). DGM-Information-Ges., Oberursel 1986, 115-123 (ISBN 3-88355-101-5)

[3] J. Pospiech: The smoothing of the orientation distribution density introduced by calculation methods. Textures and Microstructures **26-27** (1996) 83-91

## 5. The Microstructure Function

The meso- and microstructure of a polycrystal is described by the distributions of size, shape, arrangement, orientation and defects of its constituent grains and phases in three-dimensional space. A mathematical quantification of this state is given by the Microstructure Function  $G$  [1] (also named Aggregate Function) [2, 3]:

$$G(\mathbf{r}) = \begin{cases} i(\mathbf{r}) & \text{phases} \\ g(\mathbf{r}) & \text{orientations} \\ D(\mathbf{r}) & \text{defects, lattice strain.} \end{cases}$$

The phases  $i$ , the crystal orientations  $g$  and the lattice defects  $D$  in the volume elements are specified at the places  $\mathbf{r} = \{x, y, z\}$  in the specimen.  $g = \{\varphi_1, \Phi, \varphi_2\}$  are the orientation parameters,  $D = \{d_1, d_2, \dots, d_n\}$  the substructure parameters, and  $i = \{i_1, i_2, \dots, i_n\}$  the phases which are characterized by their crystal lattice and element composition.

In the simplest case, that is a single-phase material without considering the grain substructure, the microstructure function  $G(\mathbf{r})$  still depends on six coordinates that are the three spatial and the three orientation parameters. They make up a six-dimensional space which is almost beyond human imagination. So a split was made in traditional materials science by either emphasizing the morphology of microstructure or the density of grain orientations. Two branches of science have developed almost without mutual interaction:

- Stereology or Quantitative Metallography which is based on microscopy techniques to describe the morphology and phases, but with omission of the grain orientations.
- Crystal Texture Analysis which until recently was based on pole-figure measurement by diffraction methods without considering the spatial coordinates.

It is a unique feature of orientation microscopy in the SEM that this technique enables the acquisition of the microstructure function at a high spatial resolution with reasonably low effort: Scanning across the specimen surface in a raster grid yields two spatial coordinates  $\{x, y\}$  of the measured location. The third dimensional coordinate  $\{z\}$  can be obtained in principle by serial sectioning. The grain orientation,  $g$ , is the prime objective of orientation microscopy and readily available along with  $\{x, y\}$ . Phases are described by their crystal lattice. Additional information about the local element composition, e.g., from a simultaneous EDS analysis, may be helpful in phase discrimination to rule out less likely phases before performing the lattice check. Pattern quality is a (qualitative) measure of local dislocation density and lattice strain. To enable a comprehensive orientation-stereological interpretation of the microstructure, pattern quality, confidence index, and the concentrations of several elements (if measured simultaneously by EDS) are stored along with the grain orientation data for every point  $(x, y)$ .

With the availability of automated EBSD the route is now open to a comprehensive "Orientation Stereology" by merging both aspects of microstructure [1].

Depending on the application under consideration, several special functions may be derived from the universal microstructure function  $G(\mathbf{r})$  which are either sections through the six-dimensional space or integrals of it. Texture descriptors are the Orientation Density Function (ODF),  $f(g)$ , pole figures, the MisOrientation Distribution Function (MODF), orientation correlation functions, and texture fields. Of particular interest for applications in industry are tensorial materials properties that can be calculated from orientation data if the anisotropy of the property is known for the single crystalline material [4].

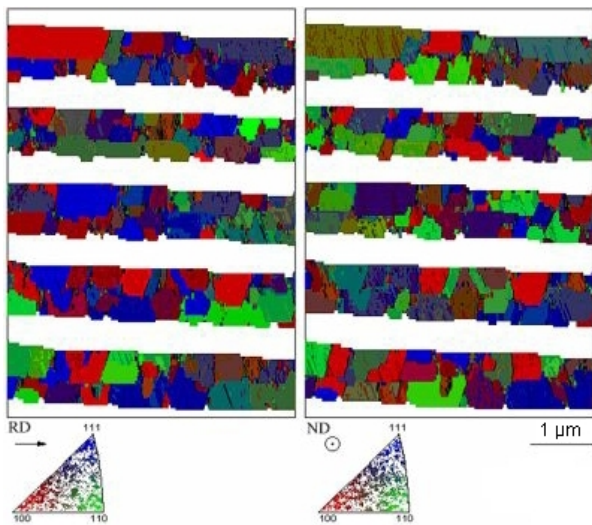
[1] H.J. Bunge and R.A. Schwarzer: Orientation stereology - A new branch in texture research. Adv. Engin. Materials **3** (2001) 25-39

[2] H.J. Bunge: Texture, microstructure and properties of polycrystalline materials. In: R.K. Ray and A.K. Singh (eds.): Texture in Materials Research, Oxford & IBH Publishing Co., New Delhi 1999, 3-44 (ISBN 81-204-1312-1)

[3] H.J. Bunge: Texture and structure of polycrystals. In: R.L. Snyder, J. Fiala and H.J. Bunge (eds): Defect and Microstructure Analysis by Diffraction, Oxford University Press, New York 1999, 405 -531 (ISBN 0-19-850189-7)

[4] H.-J. Bunge: Texture analysis in materials science - Mathematical methods. Butterworths London 1982 (ISBN 0-408-10642-5)

## 6. Electromigration failures in copper interconnect lines



About 1  $\mu\text{m}$  thick copper layers have been electroplated on trench-structured  $\text{SiO}_2/\text{Si}$  substrates by the damascene technique. The trenches were 1.0  $\mu\text{m}$  wide, 0.5  $\mu\text{m}$  deep and PVD coated with 50 nm Ta as a barrier layer to protect the silicon semiconductor from diffused copper. In addition, a PVD copper seed layer has been deposited at 50  $^\circ\text{C}$ . After the electroplating process the wafers were annealed for 10 min. at 120  $^\circ\text{C}$ . Finally the continuous copper layer has been removed by chemical-mechanical polishing (CMP) down to the damascene trenches to achieve narrow interconnect lines with sharp edges.

In the crystal orientation maps the grains are clearly discriminated from each other. Some twin grains are seen. It is worth mentioning that individual grains are hardly recognized in conventional SEM micrographs, since orientation contrast with backscatter and secondary electrons is low. A fragmented central seam of grain boundaries has formed.

The ODF and pole figures have been calculated with the series expansion method from the measured crystal orientations, separately for those grains which fill an interconnect line at full width ("bamboo grains") and for those grains which form the central seam. For both types of grain, a strong  $\langle 111 \rangle$  and a weak  $\langle 115 \rangle$  fiber texture have been found. For the bamboo grains, the fiber axes are aligned in specimen normal direction, i.e. from the bottom to the top of the trenches, whereas for the seam-forming grains the fiber axes are directed perpendicular to the sidewalls.

Since  $\langle 111 \rangle$  is the direction of fast grain growth and  $\langle 115 \rangle$  is the twin component to  $\langle 111 \rangle$  in copper, texture analysis has revealed competing columnar grain growth from the bottom and from the sidewalls of the trenches. A variety of general grain boundaries is so formed. By additives to the electrolytic bath and appropriate electroplating conditions, crystal growth from the sidewalls can be suppressed in favor of grain growth from the bottom. Seamless interconnect lines are then obtained.

A. Huot, A.H. Fischer, A. von Glasow and R.A. Schwarzer: Quantitative texture analysis of Cu damascene interconnects. In: O. Kraft, E. Arzt, C.A. Volkert, P. Ho and H. Okabayashi (Eds.): Proc. 5th Intern. Workshop on Stress-Induced Phenomena in Metallization, MPI Stuttgart 1999. AIP Conference Proceedings 491, Melville N.Y. 1999, pp. 261-264 (ISBN 13-9781563969041, ISBN 10-1563969041)

## 7. Gentle sample preparation of metals and ceramics for EBSD

The first requirement for electron microscopy is to have samples that are **stable in a vacuum** and **under the impact of high-energy electrons**. They must possess a minimum of **electrical conductivity** so as not to become charged [1]. The usual surface coating with a layer of sputtered gold, as in conventional imaging, is contraindicated for EBSD due to the shallow interaction depth of primary and diffracted electrons. Extremely thin carbon films on a grid-like support can serve as grounded conductors. Electric charge can be avoided in a variable-pressure SEM with moderate vacuum down to a few pascals, or with a gas jet in the sample chamber.

SEM EBSD is performed on solid samples. The main requirements are a **flat, clean surface, free from preparation artifacts** such as accidental deformation, reaction layers or phase-selective etching. Electro-chemical mechanical polishing (ECMP) [2] is often a good choice for **metal samples**, in particular if supported by placing the sample at positive potential of some 10 V during mechanical polishing with a suitable electrolyte. A finish by ion polishing (e.g.  $\text{Ar}^+$  at about 1 keV and flat angle of incidence) may be advisable to remove residues and oxide layers from the preparation steps. Ga from a FIBing treatment, however, tend to segregate at grain boundaries in Al and Mg samples.

At present, EBSD is mainly used for metal samples. Non-conductors, **ceramics** and sensitive samples require special treatment. They are often brittle or decompose under the electron beam. The preparation of a clean and flat surface is crucial: charging and cathodoluminescence (which can interfere with the electron detector) are a challenge.

Parasitic magnetic fields and surface contamination, i.e. an unwanted surface layer due to hydrocarbons from polymerized residual gas in the sample chamber, are problematic. Foreign layers weaken and obscure the diffraction patterns, while deformation layers broaden the Kikuchi bands, resulting in diffuse patterns. All this has a negative effect on the accuracy of the indexing.

It is far less tedious to prepare a suitable bulk sample for EBSD than a thin electron-transparent film for TKD. In any case, **sample preparation is the most important factor in optimizing performance**.

[1] R.A. Schwarzer: *Preparation of high-resistance or sensitive samples for grain orientation measurement with electron*

microscopes. Materials Science Forum **157-162** (1994) 201-206

[Download](#)  [2] R.A. Schwarzer: *The preparation of Mg, Cd and Zn samples for crystal orientation mapping with BKD in an SEM*. Microscopy Today **15**/March (2007) 40, 42

[3] J.K. Farrer, J.R. Michael and C.B. Carter: *EBSD of ceramic materials*. Chapt. 24, p. 299 - 318. in: A.J. Schwartz, M. Kumar and B.L. Adams (eds.): *Electron Backscatter Diffraction in Materials Science*. Kluwer Academic / Plenum Publishers, New York 2000

ISBN 0-306-46487-X [https://doi.org/10.1007/978-1-4757-3205-4\\_24](https://doi.org/10.1007/978-1-4757-3205-4_24)

Home

Basics

TKD

Radon vs Hough

FastEBSD

Conclusions

Publications

Downloads

Glossary